Published in final edited form as:
Magn Reson Imaging. 2012 April ; 30(3): 323–329. doi:10.1016/j.mri.2011.12.004.

Variations in T2* and Fat Content of Murine Brown and White Adipose Tissues by Chemical-Shift MRI

Houchun H. Hu, Ph.D.[1], **Catherine D.G. Hines, Ph.D.**[2,4], **Daniel L. Smith Jr., Ph.D.**[3], and **Scott B. Reeder, M.D., Ph.D.**[4,5,6,7]

[1]Department of Radiology, Children's Hospital Los Angeles, Los Angeles, California

[2]Imaging Department, Merck Research Laboratories, West Point, Pennsylvania

[3]Department of Nutrition Science, University of Alabama at Birmingham

[4]Department of Radiology, University of Wisconsin-Madison

[5]Department of Medical Physics, University of Wisconsin-Madison

[6]Department of Biomedical Engineering, University of Wisconsin-Madison

[7]Department of Medicine, University of Wisconsin-Madison

Abstract

Purpose—To compare T_2* relaxation times and proton density fat-fraction (PDFF) values between brown (BAT) and white (WAT) adipose tissue in lean and ob/ob mice.

Materials and Methods—A group of lean male mice (n=6), and two groups of ob/ob male mice placed on similar four-week (n=6) and eight-week (n=8) *ad libitum* diets, were utilized. The animals were imaged at 3 Tesla using a T_2*-corrected chemical-shift based water-fat MRI method that provides simultaneous estimation of T_2* and PDFF on a voxel-wise basis. Regions of interest were drawn within the interscapular BAT and gonadal WAT depots on co-registered T_2* and PDFF maps. Measurements were assessed using analysis of variance, Bonferroni-adjusted *t*-test for multi-group comparisons, and the Tukey post-hoc test.

Results—Significant differences ($p<0.01$) in BAT T_2* and PDFF were observed between the lean and ob/ob groups. The ob/ob animals exhibited longer BAT T_2* and greater PDFF than lean animals. However, only BAT PDFF was significantly different ($p<0.01$) between the two ob/ob groups. When comparing BAT to WAT within each group, T_2* and PDFF values were consistently lower in BAT than WAT ($p<0.01$). The difference was most prominent in the lean animals. In both ob/ob groups, BAT exhibited very WAT-like appearances and properties on the MRI images.

Conclusion—T_2* and PDFF are lower in BAT than WAT. This is likely due to variations in tissue composition. The values were consistently lower in lean mice than in ob/ob mice, suggestive of the former's greater demand for BAT thermogenesis and reflective of leptin hormone deficiencies and diminished BAT metabolic activity in the latter.

Corresponding Author Houchun Harry Hu, Children's Hospital Los Angeles, 4650 Sunset Boulevard, MS #81, Los Angeles, California, USA 90027, Phone: 323-361-2688, Fax: 323-361-1510, houchunh@usc.edu, hhu@chla.usc.edu.

Keywords

Brown adipose tissue; white adipose tissue; T_2* relaxation; fat fraction

INTRODUCTION

In rodents, brown adipose tissue (BAT) contributes to thermal regulation and energy balance [1, 2]. Many literature reports have investigated the tissue's physiology in animals and humans [3–24]. The activity of this tissue and its relation to metabolism has led to implications of BAT as a preventive mechanism against weight gain and obesity. In contrast to white adipose tissue (WAT), which functions to store energy in the form of lipids, BAT, when activated by the sympathetic nervous system, metabolizes fatty acids and carbohydrates to generate heat. The heat maintains core body temperature during prolonged cold exposure as a form of non-shivering thermogenesis (e.g. hibernation) and the expended energy can easily account for more than 50% of the total energy metabolism in small mammals [9]. BAT is also believed to facilitate dissipation of energy from excess food intake, a process known as diet-induced thermogenesis. Whereas WAT is characterized by large adipocytes that contain a unilocular intracellular lipid droplet and limited cytoplasm, BAT usually contains smaller adipocytes with multiple intracellular fat droplets, replete with iron-rich mitochondria organelles and a more extensive cytoplasm [25]. BAT is also densely vascularized as blood perfusion is needed to supply nutrients during prolonged activation and thermogenesis, as well as to transport the produced heat throughout the body [9, 11, 24, 26].

In the vast majority of animal studies to date, characterization of BAT is performed *ex vivo* by histology, after the animal has been euthanized and the tissue has been dissected. Recent works have demonstrated tissue signal contrast between BAT and WAT in mice with non-invasive MRI, using spectroscopy and chemical shift water-fat imaging techniques. These approaches have exploited morphological differences between BAT and WAT to identify unique spectral interactions [19], proton density fat-fraction (PDFF) [27, 28], T_1 relaxation times [29], and triglyceride unsaturation [29, 30]. Therefore, quantitative MRI can potentially be a non-invasive platform for detection and characterization of BAT *in vivo*.

The purpose of this work was to investigate whether T_2* differences between BAT and WAT can be measured by quantitative MRI. We hypothesize that the presence of blood flow in BAT and its greater mitochondria content [31] should lead to detectable differences in *in vivo* T_2* relaxation rates in contrast to WAT. We also suspect that in mice with greater BAT stimulation and thermogenic activity/capacity, the associated T_2* will be lower than in animals with suppressed or metabolically inactive BAT.

MATERIALS and METHODS

Animals

All animal procedures were approved by the local Institutional Animal Care and Use Committee at the University of Wisconsin. We chose the ob/ob mouse as a model with impaired thermogensis. It is a well-established model for obesity, fatty liver disease, diabetes, and the metabolic syndrome [32, 33]. The ob/ob mouse is deficient in the leptin hormone, and consequently develops hyperphagia and obesity [34]. Leptin is thought to mediate signaling of BAT diet-induced thermogenesis in response to excessive food intake. In ob/ob mice, this leptin-BAT pathway is believed to be impaired [9].

Three groups of C57BL/6 male mice were prepared in this study, consisting of a wild-type lean control group (n=6), a group of ob/ob mice that were fed for four weeks (n=6), and another group of ob/ob mice that were fed for eight weeks (n=8). These three groups will subsequently be referred to as lean, obese-4, and obese-8, respectively. The mice were obtained from Harlan Laboratories (Madison, WI, USA), and were fed *ad libitum* the same rodent chow (catalog #8604 from Harlan Teklad), which contained 14% calories from fat. All mice were housed two to three animals per cage based on body weight, at an ambient temperature of 23°C, on 12-hour light/dark cycles. At the time of MRI, the lean, obese-4, and obese-8 mice were approximately 9.8, 5, and 9.7 weeks of age, respectively, and their body weights were 25.5±1.77g, 24.5±1.49g, and 43.9±5.35g.

All mice were sedated with intraperitoneal injections of 40 mg/kg body weight sodium pentobarbital (Nembutal, Ovation Pharmaceuticals, Inc., Deerfield, IL, USA). No inhaled anesthetics were used. Animals were kept on heating pads prior to imaging. However, no heat source was provided during the MRI scan. Thus, animals were off the heating pads for approximately 30 minutes. Heart and respiratory rates, and body core temperature were not monitored in this study.

MRI

We utilized an investigational version of the IDEAL (Iterative Decomposition of fat and water with Echo Asymmetry and Least squares estimation) pulse sequence. IDEAL is a chemical-shift water-fat separation technique that produces co-registered fat, water, in-phase, and out-of-phase image series as well as quantitative T_2* and PDFF maps. The method has been validated in non-alcoholic fatty liver disease [35, 36]. One attribute of IDEAL is its ability to account for signal-confounding factors such as the multi-peak spectrum of fat [37], T_1 and noise bias [38], and correction for T_2* [39,40], as well as system imperfections such as magnetic field inhomogeneity and eddy currents [41,42]. The endpoint product is an accurate PDFF map that reflects underlying proton density ratios between fat and the sum of fat and water from 0–100%. Another attribute is a co-registered T_2* map, which is a natural by-product of the reconstruction algorithm for fat quantification. In the liver, the presence of iron shortens T_2* [43].

All MRI experiments were performed on a 3 Tesla whole-body human system (MR750, GE Healthcare, Waukesha, WI, USA), using an eight-channel wrist coil. A 3D spoiled-gradient-echo sequence was used with: coronal acquisition, TR=41.4 msec, first TE=2.6 msec, echo spacing=1.4 msec, echo train length=6, one signal average, flip angle=5° to minimize T1 bias, bandwidth = ±100 kHz, and a non-zero-interpolated voxel size of 0.47 (frequency) × 0.28 (phase) × 0.8 (slice) mm^3. Mice were scanned individually and scan time for each animal was approximately 10 minutes.

Image Analysis

The largest and most easily identifiable BAT depot in mice is the interscapular depot, which is located on the dorsal side, immediately inferior to the shoulder and fore limbs (Figure 1). It is recognized on the reconstructed water-only, fat-only, and PDFF images as a triangular or trapezoid-shaped structure [27, 28] and has been extensively described in literature [9, 11]. Four to six regions-of-interest (ROIs) were manually drawn on the PDFF and corresponding T_2* maps of interscapular BAT in each animal. Similarly, ROIs were drawn in the gonadal WAT depot of each animal. The ROIs varied in size from 1.4 to 75.6 mm^2, depending on the size of each tissue depots and the animal. The average T_2* and PDFF were computed for each animal, weighted by the corresponding ROI sizes.

Statistical Analysis

Analysis of variance (ANOVA), two-sided *t*-tests with Bonferroni correction for multi-group comparisons (3 groups), and post-hoc Tukey method were utilized, with an overall statistical significance criterion of $p < 0.01$.

RESULTS

Figure 1 illustrates separated water and fat images from a mouse in the lean group. Axial, coronal, and sagittal views are shown, highlighting the prominent interscapular BAT depot (solid arrows). The dorsal depot appears in the form of a triangle or trapezoid. In the sagittal view, the gonadal WAT depot is also highlighted (dotted arrow).

Table 1 shows ANOVA statistics, highlighting the presence of significant between-group differences in BAT PDFF, BAT T_2*, and WAT PDFF, but not WAT T_2*. Table 2 summarizes PDFF and T_2* ROI measurements. The statistics reported in Table 2 are from the Bonferroni-adjusted *t*-test for multiple comparisons. The same p-values were obtained from the Tukey test. There were statistically significant differences in BAT PDFF and T_2* when comparing the lean group to either of the two ob/ob groups ($p < 0.01$). In WAT, the nominal values appeared very similar between the three groups. Nonetheless, WAT PDFF in the lean group was significantly lower than either obese group ($p < 0.01$). BAT PDFF was the only statistically significant difference ($p < 0.01$) between obese-4 and obese-8 groups, whilst all other properties (BAT T_2*, WAT PDFF, WAT T_2*) were not different between the two ob/ob groups, even after Bonferroni adjustment.

Comparing within each group in Table 2, BAT PDFF and T_2* in the lean group were significantly lower than their counterpart gonadal WAT values ($p < 0.01$). For the obese-4 and obese-8 ob/ob groups, BAT properties were nominally closer to those of WAT, but remained significantly lower as well ($p < 0.01$). Figure 2 plots the nominal data for comparison.

Figure 3 illustrates T_2* and PDFF images of the interscapular BAT depot for the three groups. The visual differences between the lean and the two ob/ob examples are evident. Note the small body shape and near absence of WAT in the lean animal. Additionally, note that in the T_2* map of the lean and obese-4 mice, the outline of the triangular interscapular BAT depot is visible. However, such T_2* tissue contrast is visually absent in the obese-8 example.

DISCUSSION

We have demonstrated the feasibility of using quantitative chemical-shift water-fat MRI to simultaneously measure differences in T_2* and PDFF between BAT and WAT. While the PDFF difference has been previously explored [28], our current objective was to demonstrate a difference in T_2*. Present findings support T_2* as an additional dimension of tissue signal contrast between BAT and WAT. Several factors can contribute to the lower T_2* in BAT. First, brown adipocytes are rich in iron-laden mitochondria. Second and more importantly, blood perfusion and oxygen consumption in BAT increases significantly when the tissue is stimulated [31], and consequently rising levels of deoxyhemoglobin can shorten local T_2*.

Since the diet and the housing environment between the three mice groups were the same in this study, we can likely attribute the measured differences in T_2* and PDFF to metabolic differences between the animal. We consistently measured lower T_2* and PDFF in the BAT of lean mice, suggesting that the tissue was in general more metabolically active in these

animals throughout the study period. We suspect that BAT was stimulated in the form of diet-induced thermogensis as a consequence of the *ad libitum* food access. We also suspect that the lean mice were more susceptible to body heat loss as a consequence of their greater surface-volume ratio and reduced subcutaneous white adipose tissue insulation. They were more likely to experience decreases in body core temperature during the MRI scan when heating elements were not utilized. Thus it is plausible that BAT was also stimulated during the MRI exam in response to non-shivering thermogenesis.

In contrast, the BAT depots in the ob/ob groups exhibited very WAT-like properties. First, it is known that leptin-deficient ob/ob mice have reduced metabolic rates, uncontrolled appetite and food intake, unregulated satiety, and that the animals suffer from imbalances in energy regulation. This is coupled with the notion that leptin is a mediator of BAT recruitment in response to chronically increased food intake [9]. As a consequence of their leptin deficiency, we suspect that ob/ob mice may have a diminished ability to stimulate their BAT diet-induced thermogensis pathway. Second, their insulation from a thick layer of subcutaneous WAT possibly reduces their thermal sensitivity to ambient temperature, in particular during the MRI exam where heating pads were unavailable. Thus, BAT's involvement in non-shivering thermogenesis may also be suppressed.

In a recent study using computed tomography, it was shown that inactive BAT exhibits similar characteristics to WAT in the form of Hounsfield Units [44]. This supports the notion that if unused, non-stimulated BAT likely accumulates intracellular lipid stores and exhibits a more WAT-like phenotype. The potential for unilocular white adipocytes to infiltrate inactive BAT clusters is also plausible in ob/ob mice. Past literature has shown that brown adipocytes can contain varying sizes of lipid droplets, depending on the tissue's level of stimulation and activity [14, 45–47]. Brown adipocytes can further exist in small clusters amidst surrounding white adipocytes. Overall, we suspect reduced BAT activity in ob/ob mice, largely as a manifestation of their leptin deficiency and increased body adiposity.

We did not observe a correlation between the BAT PDFF and T_2*. It would be logical to speculate that BAT PDFF and T_2* would both be reduced as a function of greater tissue activity. A longitudinal study would be more appropriate to study this association, where ambient or housing temperature [48] and diet can be varied.

We recognize several limitations in this work. First, no measurements on core body temperature or energy expenditure were collected. Thus, the possibility of wild-type and ob/ob mice having different core body temperatures and the potential of this difference in affecting BAT activity can not be ignored. Second, MRI exams were only performed at the end of the feeding regimen. The availability of baseline MRI data, along with temperature and metabolic measurements, would have enhanced the interpretation of our results and strengthened the study. The acquisition of MRI data periodically throughout the feeding period should be considered in future work. Third, we recognize age as confounding factor. A previous study has shown that BAT PDFF correlates positively with age, but no associations were observed with T_2* [28].

Another limitation was the sole comparison between wild-type mice against ob/ob animals under unrestricted food access. Future studies should include animals such as a wild-type group placed on unrestricted high-fat obesogenic diet, an ob/ob group placed on restricted diet, and/or a wild-type group placed on restricted diet. Their inclusion would provide greater insight and discrimination towards the source of BAT T_2* variation. Lastly, histology was not performed in this study, but would have been useful in providing unequivocal confirmation of MRI findings. We do not anticipate BAT to be different between animal genotypes. Regardless of mouse genotype, the intrinsic thermogenic

function of BAT should not be altered, and the tissue expresses the same uncoupling protein UCP-1 and β3-adrenergic receptors. Fundamentally, we suspect it is the level of BAT stimulation by the sympathetic nervous system, the associated changes in blood perfusion and oxygen consumption, the subsequent degree of lipid and glucose combustion, and the presence of mitochondria within BAT, that leads to observed variations in T_2* and PDFF.

The use of anesthesia may suppress BAT function [50], particularly inhalants such as halothane and isoflurane. While this study utilized an injection of pentobarbital, the possibility that the measured BAT T_2* were not indicative of the full activation potential of the tissue should be recognized. The T_2* values are possibly underestimated due to decreased blood flow and oxygen exchange in comparison to normal, non-anesthetized conditions.

One technical limitation was that we utilized a pre-calibrated spectral profile based on liver fat and WAT from human data in the current IDEAL reconstruction [37, 49]. It is possible that the spectral characteristics of triglycerides in BAT are different. However, the underlying chemical composition of BAT and WAT are similar [29, 30], and although reports have shown that they vary slightly in the degree of triglyceride saturation, it is unlikely such small and subtle variations in the number of C=C and olefinic protons will significantly impact PDFF. Yokoo, et al. has demonstrated that the estimated PDFF is relatively insensitive to moderate differences in the spectral models used for fat quantification [51]. Regardless, the use of a multi-peak spectral model is most certainly more accurate than a single-resonance peak model of fat, which has been predominantly used in the past.

Another technical limitation for the estimation of T_2* is the effect of macroscopic susceptibility gradients that could act to shorten the apparent T_2*. Fortunately, this effect was largely mitigated through the use of small voxels that limited dephasing from macroscopic field inhomogeneities. Visual inspection of the magnetic field maps generated by IDEAL showed minimal field inhomogeneity variations at the locations where WAT and BAT measurements were made. The mice were also oriented along the main magnetic field direction, which should minimize gradient susceptibility effects.

In conclusion, the present work has demonstrated the feasibility of simultaneously measuring of T_2* and PDFF in BAT using quantitative chemical-shift water-fat MRI. We suspect BAT T_2* variations between wild-type and ob/ob animals were caused by a combination of effects from their genotype (e.g. leptin deficiency) and phenotype (e.g. thermogenic demand, metabolism rate). The results suggest a framework for using MRI to detect BAT *in vivo* based on relaxation parameters, PDFFs, and possibly in conjunction with perfusion pulse sequences utilizing blood-oxygenation-level-dependent contrast mechanisms. Such combinatorial approach is attractive to longitudinally assess BAT alterations in response to environmental manipulations and under acute stimulated and suppressed conditions [48].

Acknowledgments

Grant Support

National Institutes of Health

HH - K25DK087931

DS – P30DK56336

SR - R01DK083380, R01DK088925

References

1. Himms-Hagen J. Obesity may be due to a malfunctioning of brown fat. Can Med Assoc J. 1979; 121(10):1361–1364. [PubMed: 391377]
2. Himms-Hagen J. Thermogenesis in brown adipose tissue as an energy buffer. Implications for obesity. N Engl J Med. 1984; 311(24):1549–1558. [PubMed: 6390200]
3. Virtanen KA, Lidell ME, Orava J, Heglind M, Westergren R, Niemi T, Taittonen M, Laine J, Savisto NJ, Enerback S, Nuutila P. Functional brown adipose tissue in healthy adults. N Engl J Med. 2009; 360(15):1518–1525. [PubMed: 19357407]
4. Nedergaard J, Cannon B. The changed metabolic world with human brown adipose tissue: therapeutic visions. Cell Metab. 2010; 11(4):268–272. [PubMed: 20374959]
5. Kozak LP. Brown fat and the myth of diet-induced thermogenesis. Cell Metab. 2010; 11(4):263–267. [PubMed: 20374958]
6. Au-Yong IT, Thorn N, Ganatra R, Perkins AC, Symonds ME. Brown adipose tissue and seasonal variation in humans. Diabetes. 2009; 58(11):2583–2587. [PubMed: 19696186]
7. Enerback S. Human brown adipose tissue. Cell Metab. 2010; 11(4):248–252. [PubMed: 20374955]
8. Trayhurn P, Jones PM, McGuckin MM, Goodbody AE. Effects of overfeeding on energy balance and brown fat thermogenesis in obese (ob/ob) mice. Nature. 1982; 295(5847):323–325. [PubMed: 7057896]
9. Cannon B, Nedergaard J. Brown adipose tissue: function and physiological significance. Physiol Rev. 2004; 84(1):277–359. [PubMed: 14715917]
10. Nedergaard J, Bengtsson T, Cannon B. Unexpected evidence for active brown adipose tissue in adult humans. Am J Physiol Endocrinol Metab. 2007; 293(2):E444–452. [PubMed: 17473055]
11. Cinti S. The role of brown adipose tissue in human obesity. Nutr Metab Cardiovasc Dis. 2006; 16(8):569–574. [PubMed: 17113764]
12. Cypess AM, Lehman S, Williams G, Tal I, Rodman D, Goldfine AB, Kuo FC, Palmer EL, Tseng YH, Doria A, Kolodny GM, Kahn CR. Identification and importance of brown adipose tissue in adult humans. N Engl J Med. 2009; 360(15):1509–1517. [PubMed: 19357406]
13. Palmer EL, Tseng YH, Doria A, Kolodny GM, Kahn CR. Identification and importance of brown adipose tissue in adult humans. N Engl J Med. 2009; 360(15):1509–1517. [PubMed: 19357406]
14. Heaton JM. The distribution of brown adipose tissue in the human. J Anat. 1972; 112(Pt 1):35–39. [PubMed: 5086212]
15. Trayhurn P, Goodbody AE, James WP. A role for brown adipose tissue in the genesis of obesity? Studies on experimental animals. Proc Nutr Soc. 1982; 41(2):127–131. [PubMed: 7051011]
16. Goodbody AE, Trayhurn P. Studies on the activity of brown adipose tissue in suckling, pre-obese, ob/ob mice. Biochim Biophys Acta. 1982; 680(2):119–126. [PubMed: 7093244]
17. van Marken Lichtenbelt WD, Vanhommerig JW, Smulders NM, Drossaerts JM, Kemerink GJ, Bouvy ND, Schrauwen P, Teule GJ. Cold-activated brown adipose tissue in healthy men. N Engl J Med. 2009; 360(15):1500–1508. [PubMed: 19357405]
18. Pfannenberg C, Werner MK, Ripkens S, Stef I, Deckert A, Schmadl M, Reimold M, Haring HU, Claussen CD, Stefan N. Impact of age on the relationships of brown adipose tissue with sex and adiposity in humans. Diabetes. 2010; 59(7):1789–1793. [PubMed: 20357363]
19. Branca RT, Warren WS. In vivo brown adipose tissue detection and characterization using water-lipid intermolecular zero-quantum coherences. Magn Reson Med. 2011; 65(2):313–319. [PubMed: 20939093]
20. Vijgen GH, Bouvy ND, Teule GJ, Brans B, Schrauwen P, van Marken.
21. van Marken Lichtenbelt WD. Brown adipose tissue in morbidly obese subjects. PLoS One. 2011; 6(2):e17247. [PubMed: 21390318]
22. Virtanen KA, Nuutila P. Brown adipose tissue in humans. Curr Opin Lipidol. 2011; 22(1):49–54. [PubMed: 21157334]
23. Lecoultre V, Ravussin E. Brown adipose tissue and aging. Curr Opin Clin Nutr Metab Care. 2011; 14(1):1–6. [PubMed: 21088572]

24. Cannon B, Nedergaard J. Nonshivering thermogenesis and its adequate measurement in metabolic studies. J Exp Biol. 2011; 214(Pt 2):242–253. [PubMed: 21177944]
25. Menschik Z. Histochemical comparison of brown and white adipose tissue in guinea pigs. Anat Rec. 1953; 116(4):439–455. [PubMed: 13080688]
26. Feldmann HM, Golozoubova V, Cannon B, Nedergaard J. UCP1 ablation induces obesity and abolishes diet-induced thermogenesis in mice exempt from thermal stress by living at thermoneutrality. Cell Metab. 2009; 9(2):203–209. [PubMed: 19187776]
27. Sbarbati A, Guerrini U, Marzola P, Asperio R, Osculati F. Chemical shift imaging at 4. 7 Tesla of brown adipose tissue. J Lipid Res. 1997; 38(2):343–347. [PubMed: 9162753]
28. Hu HH, Smith DL Jr, Nayak KS, Goran MI, Nagy TR. Identification of brown adipose tissue in mice with fat-water IDEAL-MRI. J Magn Reson Imaging. 2010; 31(5):1195–1202. [PubMed: 20432356]
29. Hamilton G, Bydder M, Smith DL Jr, Nayak KS, Hu HH. Properties of brown and white adipose tissue measured by 1H MRS. J of Magn Reson Imaging. 2011; 34(2):468–473. [PubMed: 21780237]
30. Lunati E, Marzola P, Nicolato E, Fedrigo M, Villa M, Sbarbati A. In vivo quantitative lipidic map of brown adipose tissue by chemical shift imaging at 4. 7 Tesla. J Lipid Res. 1999; 40(8):1395–1400. [PubMed: 10428975]
31. Foster DO, Frydman ML. Tissue distribution of cold-induced thermogenesis in conscious warm- or cold-acclimated rats reevaluated from changes in tissue blood flow: the dominant role of brown adipose tissue in the replacement of shivering by nonshivering thermogenesis. Can J Physiol Pharmacol. 1979; 57(3):257–270. [PubMed: 445227]
32. Menahan LA. Age-related changes in lipid and carbohydrate metabolism of the genetically obese mouse. Metabolism. 1983; 32(2):172–178. [PubMed: 6338347]
33. Nanji AA. Animal models of nonalcoholic fatty liver disease and steatohepatitis. Clin Liver Dis. 2004; 8(3):559–574. ix. [PubMed: 15331064]
34. Trayhurn P. Biology of leptin--its implications and consequences for the treatment of obesity. Int J Obes Relat Metab Disord. 2001; 25 (Suppl 1):S26–28. [PubMed: 11466582]
35. Meisamy S, Hines CD, Hamilton G, Sirlin CB, McKenzie CA, Yu H, Brittain JH, Reeder SB. Quantification of hepatic steatosis with T1-independent, T2-corrected MR imaging with spectral modeling of fat: blinded comparison with MR spectroscopy. Radiology. 2011; 258(3):767–775. [PubMed: 21248233]
36. Hines CD, Yu H, Shimakawa A, McKenzie CA, Brittain JH, Reeder SB. T1 independent, T2* corrected MRI with accurate spectral modeling for quantification of fat: validation in a fat-water-SPIO phantom. J Magn Reson Imaging. 2009; 30(5):1215–1222. [PubMed: 19856457]
37. Yu H, Shimakawa A, McKenzie CA, Brodsky E, Brittain JH, Reeder SB. Multiecho water-fat separation and simultaneous R2* estimation with multifrequency fat spectrum modeling. Magn Reson Med. 2008; 60(5):1122–1134. [PubMed: 18956464]
38. Liu CY, McKenzie CA, Yu H, Brittain JH, Reeder SB. Fat quantification with IDEAL gradient echo imaging: correction of bias from T1 and noise. Magn Reson Med. 2007; 58(2):354–364. [PubMed: 17654578]
39. Chebrolu VV, Hines CD, Yu H, Pineda AR, Shimakawa A, McKenzie CA, Samsonov A, Brittain JH, Reeder SB. Independent estimation of T2* for water and fat for improved accuracy of fat quantification. Magn Reson Med. 2010; 63(4):849–857. [PubMed: 20373385]
40. Reeder SB, Bice EK, Yu H, Hernando D, Pineda AR. On the performance of T2* correction methods for quantification of hepatic fat content. Magn Reson Med. 201110.1002/mrm.23016
41. Yu H, Shimakawa A, Hines CD, McKenzie CA, Hamilton G, Sirlin CB, Brittain JH, Reeder SB. Combination of complex-based and magnitude-based multiecho water-fat separation for accurate quantification of fat-fraction. Magn Reson Med. 2011; 66(1):199–206. [PubMed: 21695724]
42. Hernando D, Hines CD, Yu H, Reeder SB. Addressing phase errors in fat-water imaging using a mixed magnitude/complex fitting method. Magn Reson Med. 201110.1002/mrm.23044
43. Vasanawala SS, Yu H, Shimakawa A, Jeng M, Brittain JH. Estimation of liver T*(2) in transfusion-related iron overload in patients with weighted least squares T*(2) IDEAL. Magn Reson Med. 201110.1002/mrm.22986

44. Baba S, Jacene HA, Engles JM, Honda H, Wahl RL. CT Hounsefield units of brown adipose tissue increase with activation: preclinical and clinical studies. J Nucl Med. 2010; 51:246–250. [PubMed: 20124047]
45. Tanuma Y, Tamamoto M, Ito T, Yokochi C. The occurrence of brown adipose tissue in perirenal fat in Japanese. Arch Histol Jpn. 1975; 38(1):43–70. [PubMed: 1200786]
46. Barbatelli G, Murano I, Madsen L, Hao Q, Jimenez M, Kristiansen K, Giacobino JP, De Matteis R, Cinti S. The emergence of cold-induced brown adipocytes in mouse white fat depots is determined predominantly by white to brown adipocyte transdifferentiation. Am J Physiol Endocrinol Metab. 2000; 298(6):E1244–1253. [PubMed: 20354155]
47. Petrovic N, Walden TB, Shabalina IG, Timmons JA, Cannon B, Nedergaard J. Chronic peroxisome proliferator-activated receptor gamma (PPARgamma) activation of epididymally derived white adipocyte cultures reveals a population of thermogenically competent, UCP1-containing adipocytes molecularly distinct from classic brown adipocytes. J Biol Chem. 2010; 285(10):7153–7164. [PubMed: 20028987]
48. Hu HH, Smith DL, Goran MI, Nagy TR, Nayak KS. Characterization of brown adipose tissue in mice with IDEAL fat-water MRI. Proceedings of the International Society for Magnetic Resonance in Medicine. 2010:749.
49. Hamilton G, Yokoo T, Bydder M, Cruite I, Schroeder ME, Sirlin CB, Middleton MS. In vivo characterization of the liver fat (1)H MR spectrum. NMR Biomed. 2011; 24(7):784–790. [PubMed: 21834002]
50. Ohlson KB, Lindahl SG, Cannon B, Nedergaard J. Thermogenesis inhibition in brown adipocytes is a specific property of volatile anesthetics. Anesthesiology. 2003; 98(2):437–448. [PubMed: 12552204]
51. Yokoo T, Bydder M, Hamilton G, Middleton MS, Patton HM, Hassanein T, Schwimmer J, Sirlin CB. Effects of fat spectral model parameters on hepatic fat quantification by multi-echo gradient-echo magnetic resonance imaging. Proceedings of the International Society for Magnetic Resonance in Medicine. 2009:2134.

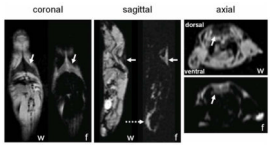

Figure 1.

Coronal, sagittal, and axial water (w)-only and fat (f)-only images in a lean mouse. Solid arrows highlight the interscapular BAT depot that resides on the dorsal side of the animal, inferior to the shoulder and fore limbs. In the coronal and sagittal views, the depot appears triangular in shape. In the axial view, the unique trapezoid shape is also unmistakable along the posterior (dorsal, top edge of image) side of the animal. Dotted arrow points to the gonadal WAT depot located on the ventral side of the animal.

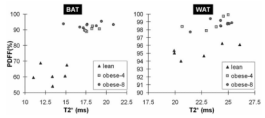

Figure 2.
Scatter plots of T_2* and PDFF for interscapular BAT (left) and gonadal WAT (right) for the lean, obese-4, and obese-8 mice groups. Note the vertical PDFF scale of the WAT plot.

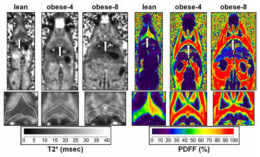

Figure 3.

Coronal single slices illustrating differences in T_2* and PDFF between the three mice groups. Arrows in each pair of images point to the same BAT location. Note that the triangular shape of the interscapular BAT depot is clearly visible in all three PDFF maps. However, based on the signal contrast in the T_2* maps, the depot is only visually identifiable in the lean and obese-4 examples. It is indistinguishable from surrounding tissues in the obese-8 example. Note the near absence of WAT in the lean mouse. Enlargements of the BAT depot are also shown along the bottom row, with a white outline drawn about the perimeter on the T_2* maps.

Table 1

ANOVA results for PDFF and T2* measurements across the three mice groups.

	BAT		WAT	
	PDFF	**T_2***	**PDFF**	**T_2***
ANOVA *F* statistic	191.3	19.5	50.6	1.82
p-value	$p < 0.01$	$p < 0.01$	$p < 0.01$	NS

Table 2

Mean (standard deviation) of PDFF and T_2* measurements of interscapular BAT and gonadal WAT. Statistics computed based on two sample two-sided *t* test with Bonferroni correction for multiple comparisons. Tukey post-hoc analysis yielded the same group-wise p-values.

	BAT		WAT	
	PDFF (%)	**T_2* (msec)**	**PDFF (%)**	**T_2* (msec)**
lean (n = 6)	61.8 (±5.5)	13.3 (±1.6)	95.2 (±0.9)	22.3 (±2.6)
obese-4 (n = 6)	90.2 (±1.2)	18.0 (±0.7)	98.8 (±0.8)	23.7 (±1.7)
obese-8 (n = 8)	93.0 (±1.3)	17.9 (±1.8)	98.7 (±0.5)	24.1 (±1.2)
lean vs. obese-4	$p < 0.01$	$p < 0.01$	$p < 0.01$	NS
lean vs. obese-8	$p < 0.01$	$p < 0.01$	$p < 0.01$	NS
obese-4 vs. obese-8	$p < 0.01$	NS	NS	NS